Mechanism of Ion Transport in Amorphous Poly(ethylene oxide)/ LiTFSI from Molecular Dynamics Simulations

Oleg Borodin*,† and Grant D. Smith†,‡

Department of Materials Science & Engineering, 122 S. Central Campus Dr, Rm 304, University of Utah, Salt Lake City, Utah 84112-0560, and Department of Chemical Engineering, University of Utah, Salt Lake City, Utah 84112-0560

Received October 21, 2005; Revised Manuscript Received December 7, 2005

ABSTRACT: The mechanisms of lithium cation (Li^+) and bis(trifluoromethane)sulfonamide anion ($TFSI^-$) transport in poly(ethylene oxide) (PEO, $M_w = 2380$) melts were examined using molecular dynamics (MD) simulations over a wide range of salt concentrations and temperatures. MD simulations using a quantum-chemistry-based many-body polarizable force field yielded ion self-diffusion coefficients, electrolyte conductivity, ion aggregation, and the coordination environment of Li^+ in good agreement with experiment. Lithium transport was found to arise from a combination of the subdiffusive Li^+ motion along PEO chains, motion together with PEO segments and intersegmental Li^+ hops from one PEO segment to another. The rate of intersegmental hops was found to correlate well with times at which Li^+ motion crosses over from subdiffusive to diffusive behavior. The contribution of Li^+ motion along PEO chains to the total Li^+ transport was found to be approximately equal to the contribution from Li^+ moving together with PEO segments. Diffusion of both Li^+ and $TFSI^-$ was found to be strongly coupled to PEO ether oxygen atom displacements and PEO conformational dynamics.

I. Introduction

Lithium secondary batteries are primary candidates for use in electric and hybrid-electric vehicles. Use of lithium metal as an anode material offers the highest theoretical energy density for secondary lithium batteries. Unfortunately, liquid electrolytes cannot be used with the lithium metal anode because of dendrite growth during charge−discharge.[1] Solid polymer electrolytes (SPE) formed by dissolving lithium salts in a polymer matrix exhibit significantly slower dendrite growth or can inhibit it completely. They also combine ease of fabrication, good electrochemical stability, low flammability, and toxicity with the ability to form good interfacial contact with electrodes during charge−discharge cycles and eliminate a need for a separator.[2] Despite many advantages over liquid electrolytes, SPEs exhibit low ambient temperature conductivity and low transference numbers, preventing them from being used in batteries for consumer electronics and automotive applications.[3]

The first suggested SPE's consisted of linear PEO doped with lithium salts. Many variations of the polymer chemistry and architecture have been explored including introduction of oxymethylene groups in the PEO chain,[4,5] use of block copolymers,[6] use of comb-branch polymers,[5,7] radiation cross-linking of PEO,[8] and addition of nanoparticles.[9,10] Years of extensive investigations of SPEs have led to important insight into the structure and transport characteristics of these materials. Importantly, traditional lithium salts ($LiBF_4$, $LiPF_6$, Li-triflate) have been found to aggregate extensively in SPE matrices. The extent of aggregation increases with increasing salt concentration and temperature and is found to be dependent on the size of anion. Large anions with delocalized charge tend to have lower binding to Li^+ and yield more free (uncomplexed by anion) Li^+ cations available for charge transport. The bis(trifluoromethane)sulfonamide anion ($TFSI^-$) is one of the most popular large anions, and it is shown in Figure 1. LiTFSI was found to largely dissociate in PEO matrices. While the ambient temperature conductivity of PEO-based/LiTFSI SPEs remains below acceptable levels, these materials are among the promising developed to date, and an increased fundamental understanding of cation and ion transport in PEO/LiTFSI could play an important role in development of improved SPEs.

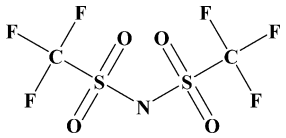

Figure 1. Structure of bis(trifluoromethane)sulfonamide ($TFSI^-$) anion.

Molecular dynamics (MD) simulations are, in principle, well suited for exploring transport mechanisms in SPEs. However, while a number of MD simulation studies of PEO-based SPEs have been reported, most could not provide reliable predictions of electrolyte conductivity and ion transport, thus prompting questions about conclusions drawn from these simulation studies regarding transport mechanisms.[11−17] Several events that can contribute to the Li^+ transport were observed in these simulation studies, namely, Li^+ moving along the PEO chains (but was not observed in ref 16), Li^+ complexing and decomplexing with anions, and Li^+ occasionally hopping from one PEO chain to another. The relative importance of these mechanisms has not been assessed and remains unclear. We previously showed[14] that cations that hopped from one PEO chain to another and/or extensively moved along PEO chains generally exhibited higher mobility that those that underwent limited hopping along PEO chains, thus indicating that hopping along PEO chains noticeably contributes to Li^+ diffusion. However, our simulations,[14] while longer than previous studies,[12,13] were not sufficiently long to allow quantification of the relative importance of various mechanisms to the Li^+ transport.

In this work we demonstrate that sufficiently long MD simulations utilizing a recently developed quantum chemistry-based many-body polarizable force field[18] can accurately predict Li^+ local environment, ion self-diffusion coefficients, and

† Department of Materials Science & Engineering.
‡ Department of Chemical Engineering.

10.1021/ma052277v CCC: $33.50
Published on Web 01/19/2006

Table 1. Length of MD Simulations, Fraction of Free Ions, Degree of Ion Uncorrelated Motion (α), and Rate of Intersegmental Hopping ($1/\tau_{\text{intersegment hop}}$)

salt concentration (EO:Li)	temp (K)	equilibration run length (ns)	production run length (ns)	fraction of free ions	α	$1/\tau_{\text{intersegment hop}}$ (ns^{-1})
39	423	5	8	0.91	0.90	0.053
39	393	3	16	0.96	0.91	
20	423	5	27	0.86	0.92	0.047
20	393	3	50	0.93	0.94	0.02
20	363	7	36	0.92	0.93	
20	333	3	10	0.92	0.95	
10	423	3	18	0.70	0.85	0.051
10	393	5	10.5	0.70	0.80	
7.5	423	3	11	0.65	0.77	0.041
7.5	393	2	7.3	0.66	0.79	

electrolyte conductivity in PEO/LiTFSI SPEs. We have chosen a relatively long PEO ($M_w = 2380$, 54 repeat units) in order to allow sufficient diffusion of Li^+ along polymer chain to occur but short enough to allow equilibration of global polymer conformation within a reasonable time frame. Moreover, ion self-diffusion and electrolyte conductivity in PEO ($M_w \approx 2500$ g/mol) are very similar to those of amorphous high molecular weight PEO-based electrolytes, indicating that the transport mechanism gleaned from our simulations using 54 repeat units PEO is expected to be similar to that in high molecular weight electrolytes. Our goal is to perform simulations that are long enough and utilize the accurate many-body polarizable force field in order to be able to provide definitive answers about a mechanism of the Li^+ and $TFSI^-$ transport in PEO/LiTFSI SPEs.

II. Molecular Dynamics Simulations Methodology

A version of the molecular dynamics simulation package Lucretius[19] that includes many-body polarization was used for all MD simulations. The three-dimensional, periodic cubic simulation cell consisted of 9 or 10 methoxy-terminated PEO ($M_w = 2380$) chains and 14, 27, 48, 65 LiTFSI, corresponding to salt concentrations of ether oxygen (EO):Li = 39, 20, 10, and 7.5, respectively. All SPEs were created in the gas phase corresponding to a cell (linear) dimension of ~150 Å. The cell was shrunk to the size corresponding to a density that yielded an average pressure of 1 atm over 1 ns at 450 K. Simulations were first performed at 423 K. After ≈30−50% of the trajectory at 423 K was generated, temperature was decreased to 393 K. After ≈30−50% of the trajectory at 393 K was generated, the temperature was decreased to 363 K. Table 1 summarizes the length of production and equilibration runs performed using NVT and NPT ensembles, respectively. A simulation box had linear dimensions ≈35−37 Å. A Nose-Hoover thermostat and a barostat[20] were used to control the temperature and pressure, while bond lengths were constrained using the Shake algorithm.[21] The Ewald summation method was used for treatment of long-range electrostatic forces between partial charges and between partial charges and induced dipoles for the many-body polarizable potential. A tapering function[22] was used for scaling the induced dipole−induced dipole interactions to zero at the cutoff of 10 Å, with scaling starting at 9 Å. A multiple time step reversible reference system propagator algorithm was employed,[23] with a time step of 0.5 fs for bonding, bending, and torsional motions, a 1.5 fs time step for nonbonded interactions within a 6.5 Å sphere, and a 3.0 fs time step for nonbonded interactions between 6.5 and 10.0 Å and the reciprocal space part of the Ewald summation.

While details of the force field development are given elsewhere,[18] here we briefly summarize main features of its development and validation. Namely, the PEO/LiTFSI force field is a part of a set of classical many-body polarizable force fields that were developed for *n*-alkanes, perfluoroalkanes, polyethers, ketones, and linear and cyclic carbonates.[18] Dipole atomic polarizability terms were used to capture many-body polarizable effects and were parametrized on the basis of molecular interactions with test charges. Partial charges were fitted to the electrostatic potential around a molecule. The repulsion−dispersion contribution to the nonbonded energy is determined on the basis of quantum chemistry dimer energies of model compounds and empirical thermodynamic liquid-state properties. Bonding and bending parameters were determined from vibrational frequencies and equilibrium geometries of model compounds. The torsional parameters were fit to obtain the best description of conformational energetics of model compounds obtained from ab initio quantum chemistry calculations. Molecular dynamics simulations with these force fields accurately predicted structural, dynamic, and transport properties of liquids and unentangled polymer melts and their solutions with LiTFSI.

III. Structural Properties

Ion aggregation in PEO/LiTFSI has been studied by Raman spectroscopy at 343 and 294 K.[24] Analysis of the 740 cm^{-1} Raman mode of $TFSI^-$ indicated an estimated fraction of complexed $TFSI^-$ anions (by Li^+) in PEO/LiTFSI of less than 7% for EO:Li > 8 and ≈24% for EO:Li = 6 at 343 and 294 K, indicating no change in ion aggregation with decreasing temperature. In MD simulations we defined a cation or anion to be free if there are no $Li\cdots N_{TFSI^-}$ approaches closer than 5 Å (the position of the minimum after the first peak of the $Li^+\cdots N$ radial distribution function). The fraction of free ions shown in Table 1 for all simulated systems agrees well with analysis of Raman spectroscopy studies.

The Li^+ cation environment in PEO/LiTFSI, EO:Li = 7.5:1 has been studied in recent neutron diffraction isotopic substitution (NDIS) experiments at 296 K.[25] NDIS experiments revealed a first Li−O structural peak at 2.1 ± 0.05 Å and 4.9 oxygen atoms in the first coordination shell of Li^+ at room temperature. Long polymer relaxation times at low temperature prevent us from obtaining an equilibrated Li^+ environment at room temperature. However, as ion aggregation of PEO/LiTFSI does not significantly change with temperature in MD simulations and Raman experiments, it is reasonable to assume that the Li^+ environment at room temperature and 393 K are similar and our results at 393 K can be compared against room temperature NDIS experiments. From analysis of MD trajectories of PEO/LiTFSI EO:Li = 7.5:1 at 393 K, we obtained the position of the first Li−O peak at 1.97 Å, in good agreement with NDIS experiments. The average number of ether oxygen and $TFSI^-$ oxygen atoms complexing a Li^+ cation[26] were 3.85 and 0.5, respectively, yielding a total of 4.6 oxygen atoms in the first coordination shell of a Li^+, again in good agreement with 4.9 oxygen atoms found coordinating a Li^+ in NDIS experiment.

A detailed analysis of Li^+ complexation revealed a number of representative Li^+ coordinations as shown in Figure 2. The most intriguing are the Li^+ coordinations shown in Figure 2a,b where Li^+ cations are complexed by two PEO helixes and ordered into structures with two and even three lithiums located 4.5−5 Å from each other. Such structures are not prevalent but are present sufficiently often (≈20 ± 10% of all Li^+ coordinations) and are observed for all salt concentrations except the lowest salt concentration studied (EO:Li = 39). The structures shown in Figure 2a,b resemble Li^+ complexation patterns observed in PEO/$LiXF_6$ (X = P, As, Sb) EO:Li = 6 crystal

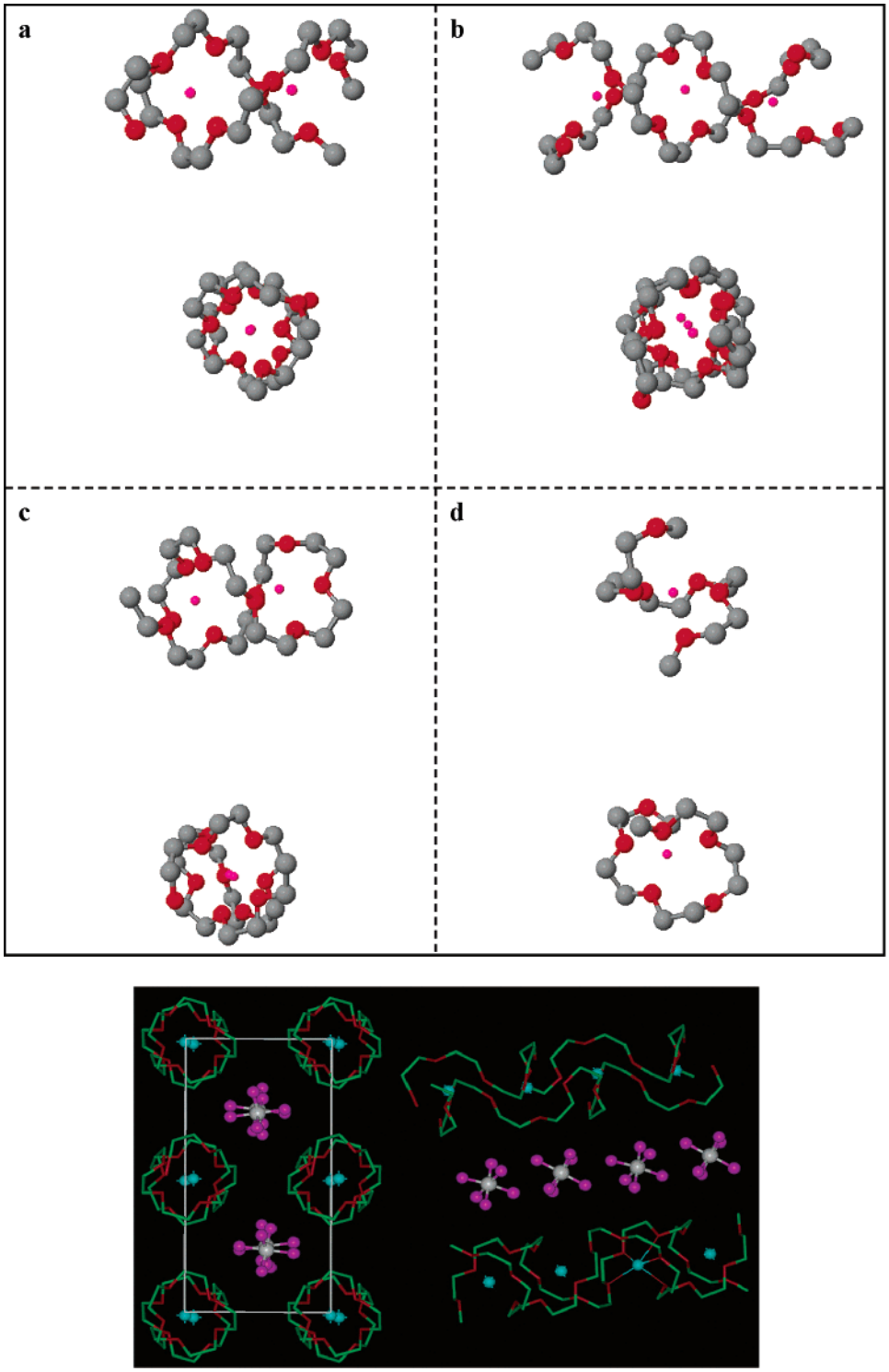

Figure 2. Snapshots from simulations of PEO/LiTFSI at 423 K (a, b, d) for EO:Li = 20:1 and (c) for EO:Li = 10:1. Hydrogen atoms are not shown for clarity. Only atoms within 4.0 Å of each Li^+ are shown. Crystal structure from X-ray diffraction measurements of PEO/$LiAsF_6$ EO:Li = 6 from ref 29 is also shown for comparison.

phases obtained from X-ray diffraction experiments by Bruce's group[27−29] and reproduced in Figure 2e for comparison. In crystal structures "the Li^+ cations are arranged in rows, with each row located inside a cylindrical surface formed by two PEO chains" (Figure 2e). The principal difference between the structures observed in MD simulations (Figure 2a,b) and those fitted to crystallographic data (Figure 2e) is that we observe a Li^+ being wrapped around by two PEO helixes, whereas fits to crystallographic data yielded Li^+ coordination by a nonhelical conformation that defines a half-cylinder. We also observed structures when a PEO chain after wrapping around two lithiums turns back to form another helix and thus complete coordination of the first Li^+, as shown in Figure 2c.

Approximately 50 ± 10% of Li^+ were complexed by two PEO segments, with the other 50% being complexed by a single PEO segment, as shown in Figure 2d for all simulated temperatures and concentrations. A segment is defined as a continuous part of a PEO chain, i.e., a set of contiguous ether oxygen atoms. For example, the Li^+ on the left in Figure 2c is complexed by two segments of the same chain, a configuration

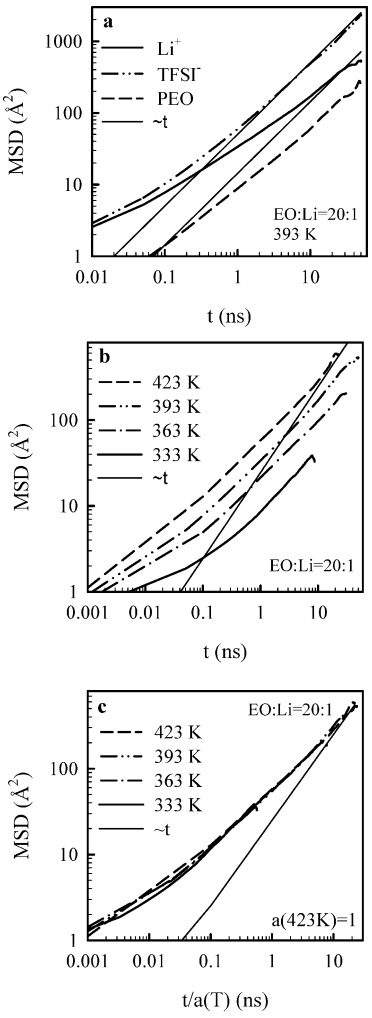

Figure 3. (a) Mean-square displacement (MSD) of Li^+, $TFSI^-$, and PEO for EO:Li = 20 at 393 K and (b, c) only Li^+ and a function of temperature. Time axis in (c) is scaled by the scaling factor $a(T)$, $a(423\ K) = 1$.

that constitutes less than 10% of Li^+ coordinations. Snapshots of a Li^+ coordinated with PEO and $TFSI^-$ anion at the same time are not shown because the frequency of their occurrence is low, and they do not follow well-defined patterns.

IV. Transport Properties

A. Ion and PEO Self-Diffusion Coefficients. The self-diffusion coefficient D is calculated using Einstein relation

$$D = \lim_{t\to\infty} D^{app}(t) = \lim_{t\to\infty} \frac{\langle MSD(t)\rangle}{6t} \qquad (1)$$

where $MSD(t)$ is mean-square displacement of a molecule center of mass during time t, $\langle\ \rangle$ denotes an ensemble average, and $D^{app}(t)$ is the time-dependent apparent diffusion coefficient. The ion and PEO MSD(t) for EO:Li = 20 at 393 K are shown in Figure 3a. The $TFSI^-$ motion is subdiffusive, i.e., $MSD(t) \sim t^{\gamma}$ with $\gamma < 1$, on subnanosecond time scale at 393 K. At times longer than a nanosecond $TFSI^-$ motion becomes diffusive, and its self-diffusion coefficient can easily be extracted by applying eq 1 directly at all temperatures. The Li^+ MSD(t) for EO:Li = 20 at 393 K is also shown in Figure 3a. The Li^+ motion is subdiffusive for up to ≈30 ns. It is necessary to reach the diffusive regime in order to accurately extract a diffusion coefficient from MD simulations. As temperature decreases, longer simulations are required in order to reach the diffusive regime, as shown in Figure 3b. Such simulations are extremely expensive especially using the many-body polarizable potentials as we employed thus posing significant difficulties in obtaining Li^+ self-diffusion coefficient at low temperatures, where Li^+ motion is subdiffusive on the scale of our simulations. However, we found that Li^+ MSD(t) at various temperatures (Figure 3b) nicely superimpose if the time axis is scaled by a temperature-dependent shift factor, $a(T)$, as shown in Figure 3c. Assuming that the same temperature-dependent shift factor that applies in the subdiffusive regime also applies in the diffusive regime, the temperature-dependent Li^+ self-diffusion coefficients are determined as

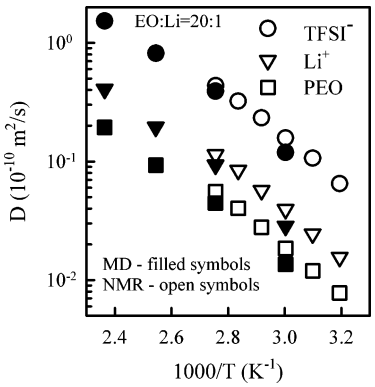

Figure 4. Self-diffusion coefficient for Li^+, $TFSI^-$, and PEO from MD simulations and pgf-NMR experiments[30] for EO:Li = 20.

$$D(T) = D(423\ K)/a(T) \qquad (2)$$

where D(423 K) was obtained utilizing eq 1 and $a(T)$ is the temperature-dependent time-shift factor obtained by superimposing Li^+ MSD(t), as shown in Figure 3b,c. As expected from previous simulations of polymer melts, at times scales less than Rouse time (time of polymer coil reorientation, ≈45 ns for EO:Li = 20 at 393 K), the PEO center of mass motion is subdiffusive ($MSD(t) \sim t^{0.8}$), as seen from Figure 3a. Nevertheless, we extracted the PEO self-diffusion coefficients utilizing eq 1 and its temperature dependence utilizing eq 2.

Figure 4 shows a comparison of the Li^+, $TFSI^-$, and PEO self-diffusion coefficients from our simulations with results of pgf-NMR experiments[30] on PEO(M_w = 2480 g/mol)/LiTFSI at EO:Li = 20. MD simulations predictions deviate by less than 30% from experiments and exhibit nearly identical temperature dependence. Similar agreement was observed for EO:Li = 10 concentration as a function of temperature (not shown). The concentration dependence of the Li^+ and $TFSI^-$ self-diffusion coefficients was measured in two pgf-NMR experiments performed on high molecular weight PEO ($M_w = 5 \times 10^6$ g/mol)[30] and lower molecular weight PEO (M_w = 2480 g/mol)[31] at 358 K. There is a noticeable difference between two sets of experimental data shown in Figure 5. This difference can be partially attributed to the difference in polymer molecular weight. We compared Li^+ and $TFSI^-$ self-diffusion coefficients extrapolated from our high temperature data for EO:Li = 39, 10, and 7.5 and interpolated for EO:Li = 20 with ion self-diffusion coefficients from pgf-NMR in Figure 5. MD simulations accurately predict decrease of the Li^+ and $TFSI^-$ self-diffusion coefficients with increasing salt concentration and are in better agreement with NMR results for the lower molecular weight PEO (M_w = 2480 g/mol) that is comparable to PEO (M_w = 2380) used in MD simulations.

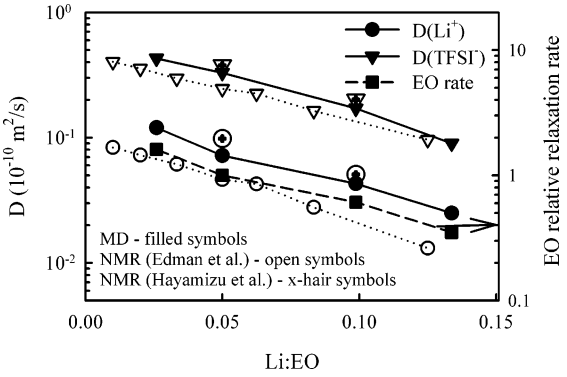

Figure 5. Concentration dependence of the Li^+, $TFSI^-$ self-diffusion coefficients from MD simulations and two pgf-NMR experiments of Edman et al.[31] and Hayamizy et al.[30] using PEO($M_w = 5 \times 10^6$ g/mol) and PEO(M_w = 2480 g/mol), respectively, at 358 K. Concentration dependence of the relative relaxation rate for EO relaxation is also shown.

B. Correlation of Ion and Polymer Motion. The diffusion coefficients obtained from simulations and pgf-NMR experiments for both Li^+ and $TFSI^-$ reveal the same decrease in diffusion coefficients upon increasing salt concentration (Figure 5). Because the salt in this electrolyte is almost completely dissociated, the decrease in cation and anion self-diffusion coefficients with increasing salt concentration is not due to ion aggregation. To check for coupling between ion motion and polymer segmental motion, we determined the concentration dependence of the characteristic rate for polymer segmental relaxation by scaling time axis of the EO MSD(t) at various concentrations in order to superimpose them. The characteristic time (inverse rate) for polymer segmental motion can also be thought of as a time for polymer backbone atoms to undergo a certain mean-square displacement, say 50 Å^2, to break out of the cage imposed by neighbor packing. The concentration dependence of the relative polymer segmental relaxation rate is also shown in Figure 5, and it is remarkably similar to concentration dependence of the diffusion coefficients of both ions, indicating that both cation and anion motion are strongly coupled to local polymer relaxation. This observation runs counter to often-used arguments[32] that anion dynamics is decoupled from those of the polymer matrix and is governed by free volume.

MD simulations offer a possibility to check how cation and anion motion is connected to segmental polymer dynamics by artificially increasing barriers for polymer conformational transitions. We performed simulations of PEO/LiTFSI EO:Li = 20:1 at 393 K with PEO backbone barriers increased by 1.3 kcal/mol for 7.5 ns and compared MSD(t) for ions from simulations using the original barriers. We found that an increase in PEO conformational barriers slowed down $TFSI^-$ and Li^+ motion by 3.2 and 2.9 times, respectively, while increasing the polymer segmental relaxation time by a factor of 3.5, clearly demonstrating that motion of both cation and anion motion are strongly coupled polymer conformational dynamics. This behavior is different from that observed for small (O_2, H_2, He, etc.) penetrant permeation, where it is believed that the primarily mechanism of motion is hopping from one preexisting free volume (void) to another without requiring substantial polymer relaxation.[33,34] Instead, the observed behavior of $TFSI^-$ is similar that observed for larger molecules in rubbery polymers[35] (e.g., bisphenol A) that show coupling of the penetrant hopping and the dynamics of the polymer matrix.

C. Electrolyte Conductivity. Ionic conductivity from MD simulations can be calculated using the Einstein relation (eq 3) provided ion motion is diffusive

$$\lambda = \lim_{t\to\infty} \frac{e^2}{6tVk_BT} \sum_{ij}^{N} z_i z_j \langle [\mathbf{R}_i(t) - \mathbf{R}_i(0)][\mathbf{R}_j(t) - \mathbf{R}_j(0)] \rangle \quad (3)$$

where e is the electron charge, V is the volume of the simulation box, k_B is Boltzmann's constant, T is the temperature, t is time, z_i and z_j are the charges over ions i and j, $\mathbf{R}_i(t)$ is the displacement of the ion i during time t, the summation is performed over all ions, $\langle\ \rangle$ denotes the ensemble average, and N is the total number of ions in the simulation box. The diagonal terms in eq 3 ($i = j$) yield contribution to ionic conduction from ion self-diffusion. Off-diagonal terms arising from cations and anions moving in the same direction (correlated ion motion) decrease the total charge transport. The degree of uncorrelated of ion motion (α) is typically measured as ratio of the collective (total) charge transport to the charge transport due to self-diffusion only (a limit of completely dissociated and uncorrelated motion) and is given by eq 4

$$\alpha = \lim_{t\to\infty} \alpha(t) = \frac{1}{(D^{\mathrm{app}}{}_{\mathrm{Li}^+} + D^{\mathrm{app}}{}_{\mathrm{TFSI}^-})N} \frac{1}{6t} \sum_{ij}^{N} z_i z_j \langle [\mathbf{R}_i(t) - \mathbf{R}_i(0)][\mathbf{R}_j(t) - \mathbf{R}_j(0)] \rangle \quad (4)$$

Thus, $\alpha = 1$ corresponds to uncorrelated ion motion, while $\alpha = 0$ if all cations move only together with anions. The ionic conductivity is also frequently expressed as

$$\lambda = \alpha Ne^2(D_+ + D_-)/Vk_BT \quad (5)$$

Equation 5 was used to obtain degree of ion correlation from a combination of pgf-NMR and conductivity measurements. Values of $\alpha = 1$ and 1.2 for PEO/LiTFSI, EO:Li = 10 and EO:Li = 20 at 333 K, respectively, were obtained, indicating complete salt dissociation. A value of 1.2 is unphysical because α cannot be greater than 1.0. The fact that it is 20% large than the physical value of 1.0 indicates the combined error bars of pgf-NMR and conductivity measurements is at least 20%.

We obtained α for PEO/LiTFSI from eq 4. The resulting degrees of uncorrelated ion motion (α) are given in Table 1. As expected from the large fraction of free ions, α is quite large and is very close to the fraction of free ions obtained from structural analysis, indicating that that motion of cations and anions separated by solvent molecules (PEO) is largely uncorrelated. Finally, the conductivity of PEO/LiTFSI was calculated from eq 5. The salt concentration dependence of the PEO/LiTFSI conductivity from MD simulations is in good agreement with results of two experimental measurements,[30,36] as seen from Figure 6.

V. Ion Transport Mechanism

Having validated the Li^+ coordination and ion transport properties for the PEO/LiTFSI SPEs predicted by MD simulations through comparison with experiment, we are now in a position to explore mechanisms of ion transport in detail. We proceed with analysis of the Li^+ transport mechanism in the following order. First, we identify possible contributions to the Li^+ transport; second, we quantify each of them and incorporate them in a microscopic model that will allow us to predict overall Li^+ transport by combining various transport mechanisms. Finally, we utilize this model to better understand the importance of each mechanism to the overall Li^+ transport.

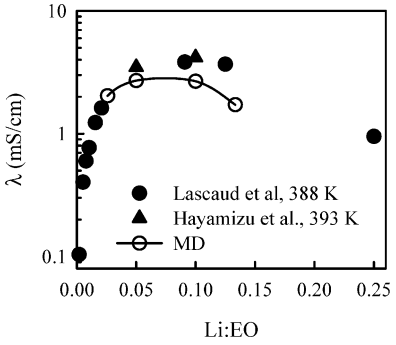

Figure 6. Concentration dependence of conductivity from MD simulations at 393 K and experiments by Lascaud et al.[36] for PEO(M_w = (3.9−4.5) × 10^3 g/mol)/LiTFSI and Hayamizy et al.[30] for PEO(M_w = 2480 g/mol)/LiTFSI.

A. Evolution of Li^+ Coordination with Time. We begin by investigation of changes in Li^+ coordination as a function of time for each Li^+. Changes in Li^+ coordination are conveniently monitored utilizing the coordination plots shown in Figure 7. Here all EO are numbered consecutively from one end of PEO chain to the other for all chains. If at any given time a Li^+ is coordinated by a specific EO, this EO is marked as a complexing EO for that cation and is shown in the plot as a filled symbol. To improve clarity of the plot and remove EO that participate in complexation for a very brief period of time, we show in Figure 7 only EO involved in complexing a Li^+ for at least 50 ps out of each 100 ps interval. Contiguous PEO segments involved in complexation of a Li^+ cation are separated from each other by dashed lines in Figure 7. Oxygen atom from $TFSI^-$ anions involved in complexing Li^+ are marked analogously to complexed EO and are shown in Figure 7.

In our simulations we observed various changes in Li^+ coordination with time that potentially can contribute to Li^+ transport. Such events can be divided into four categories: (a) A Li^+ moving along PEO chains (Figure 7a). (b) A Li^+ undergoing intersegmental hops that occur very fast (in a fraction of a nanosecond, Figure 7a at ≈ 45 ns). In our simulations most of the intersegmental Li^+ hops resulting in Li^+ changing chains and, therefore, intersegmental hops are equivalent to interchain hops. (c) Changes in Li^+ coordination from being complexed by a single PEO segment to being complexed by two PEO segments and remaining complexed by two PEO segments for multiple nanoseconds (Figure 7c, t < 4 ns and 6 ns < t < 10 ns). (d) Decomplexing from PEO segments and complexing by $TFSI^-$ anions (without PEO) with a subsequent jump to another PEO segment within a few nanoseconds. The events of types a−c were found for all electrolyte concentrations, whereas events of type d were found only for the highest salt concentrations (EO:Li = 10 and 7.5). Intriguingly, we often find a $TFSI^-$ anion approaching a Li^+ at the moment when the cation undergoes intersegmental jump as shown in Figure 7a, t ≈ 10, 42.5, and 45 ns, indicating that $TFSI^-$ anions may play an important role in promoting Li^+ intersegmental hopping. Figure 7b shows that some Li^+ cations complexed by two PEO segments for very long time (as much as our simulation time) and exhibited only quite limited motion along PEO chains. Contrasting parts a and b of Figure 7 highlights significant heterogeneity of Li^+ motion on the scale of our simulations (50 ns) as some Li^+ undergo multiple changes of its coordination, whereas others (Figure 7b) basically do not change their coordination on the scale of 50 ns at 393 K.

At the next step, we examine possible correlation between types of Li^+ coordination and Li^+ transport probed through its MSD. Figure 8 presents Li^+ MSD for the Li^+ that are complexed

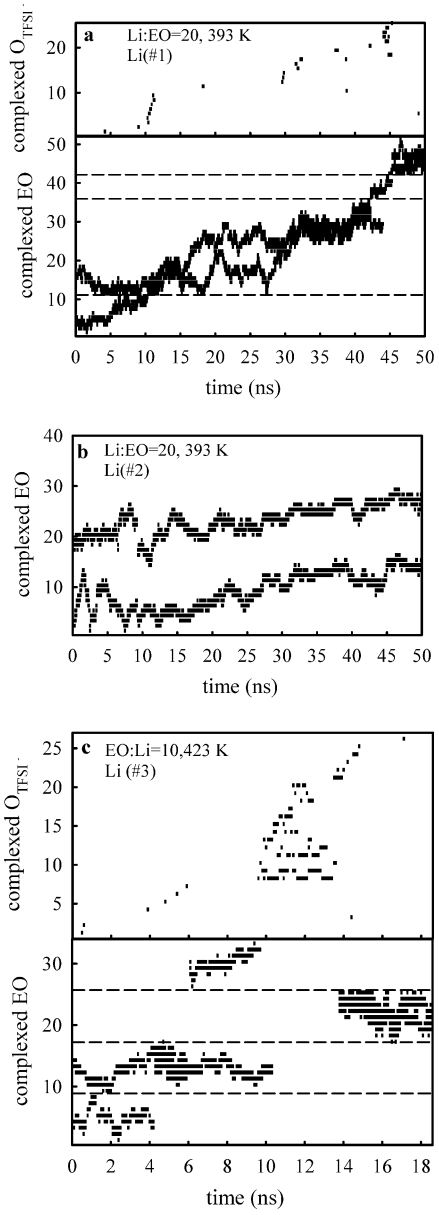

Figure 7. Plots of evolution of the Li^+ local environment with time for 3 Li^+ cations. Ether oxygen (and $TFSI^-$ oxygens) atoms complexed at each time interval of 100 ps for longer than 50 ps with a given Li^+ are marked with the filled symbol. Dashed lines separate strands of continuous ether oxygen atoms.

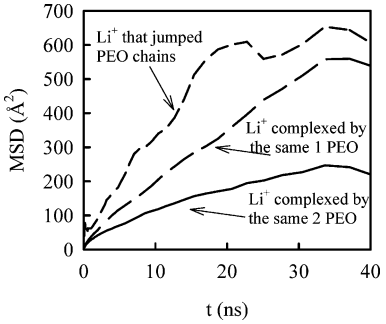

Figure 8. Mean-square displacements of the Li^+ cations that have hopped from one PEO segment to another during analysis, the Li^+ cations that were complexed by one or two PEO chains and did not undergo any intersegmental jumps during analysis for EO:Li = 20 at 393 K.

by one PEO segment and two PEO segments without undergoing intersegmental hopping during time of the analysis. We

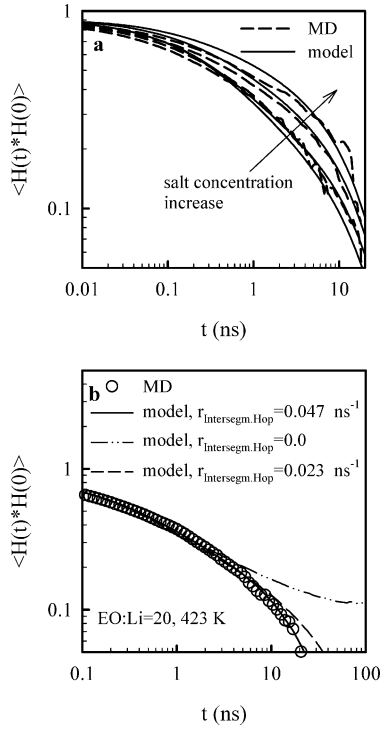

Figure 9. (a) The EO−Li^+ residence time ACF calculated directly from MD simulations and the model for Li^+ transport for EO:Li = 39, 20, 10, and 7.5 at 423 K. (b) The EO−Li^+ residence time ACF for EO:Li = 20:1 at 423 from MD and from the model with various intersegmental jump rates.

observe that on average Li^+ coordinated by two PEO segments move slower than the Li^+ coordinated by one PEO segment because Li^+ coordination by two PEOs reduces its motion along PEO chain and together with it and Li^+ cations do not move inside structures shown in Figure 2a,b that is an envisioned transport mechanism in crystalline SPEs.[28,29] The Li^+ that are complexed by one PEO segment and undergo intersegmental hops during analysis moved the fastest as seen from Figure 8.

B. Cation Motion along the Chain. We just discussed that Li^+ motion along PEO is one of mechanisms contributing to the total Li^+ transport. We do not know, however, how important this contribution is, and we wish to quantify it. It is cumbersome to count Li^+ hopping events along PEO directly as a Li^+ moves back and forth along PEO chains. However, we can easily calculate the Li^+ residence time autocorrelation function (ACF) next to ether oxygen atoms and use this information to determine the Li^+ diffusion coefficient along PEO chains. The EO−Li^+ residence ACF time is given by eq 6

$$P_{\mathrm{EO-Li}}(t) = \langle H(t)^*H(0)\rangle \qquad (6)$$

where $H(t)$ is 1 given EO has a Li^+ in its first coordination shell (2.8 Å and 0 otherwise). Representative residence time autocorrelation functions are shown in Figure 9. Integrals from zero to infinity of stretched exponential fits to the EO−Li^+ residence time autocorrelation functions yield EO−Li^+ residence times from 4.5 to 14.5 ns for EO:Li = 39 and EO:Li = 7.5 at 423 K. These residence times indicate that a Li^+ cation completely changes its coordination by ether oxygens on a 10 ns time scale at 423 K. As a Li^+ is typically coordinated by 4−5 ether oxygen atoms, we estimate that it takes ≈10 ns for a cation to move 4−5 repeat units along a PEO. The Li^+ diffusion coefficient for its motion along PEO is obtained below by applying a microscopic model of a Li^+ transport.

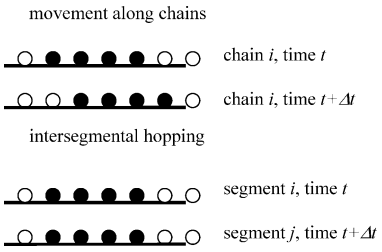

Figure 10. Two types of Li^+ motion present in a microscopic model.

C. Li^+ Transport Microscopic Model. We have developed a microscopic model for Li^+ transport that includes the underlining motional mechanisms for Li^+ transport and can reproduce the EO−Li^+ residence time distribution and Li^+ MSD(t) obtained from molecular dynamics simulations. In the model an ensemble of cations occupying coordinating sites on polymer chains is simulated, typically 150−200 Li^+. Each Li^+ occupies four coordinations sites. Each cation is allowed to move along chains containing 54 coordination sites, thus mimicking 54 repeat unit PEO. Li^+ also hops from one segment of a PEO chain to another segment of typically a different PEO chain with the probability given in Table 1 and characteristic hop length extracted from simulations and discussed below. Motion along the polymer chains as well as intersegmental (interchain) hopping is carried out utilizing Monte Carlo moves, as illustrated in Figure 10.

Two types of lithiums exist in the model: (a) free Li^+ and (b) Li^+ complexed with anions. The probability of a Li^+ to be free is taken from Table 1. Each free Li^+ is not allowed to approach another free Li^+ closer than six coordinating sites because each free Li^+ has six EO (modeled as coordinating sites) in its large (extended) coordination shell ($r_{\mathrm{Li-EO}} < 3.8$ Å). A Li^+ complexed by a TFSI anion typically has two fewer EO coordinating it; therefore, we do not allow a Li^+ complexed by an anion to approach another Li^+ complexed by another anion closer than four coordinating sites. The closest allowed approach between the complexed and free Li^+ is five coordinating sites.

The acceptance probabilities for motion of a cation along a polymer chain was varied until the EO−Li^+ residence time ACF from MD simulations and from microscopic model were in good agreement, as shown in Figure 9a. The resulting diffusion coefficients for Li^+ motion along PEO are given in Table 2. Note that it is important to include Li^+ intersegmental hopping in the microscopic model in order to be able to describe the EO−Li^+ residence time ACF at long times, because the model without Li^+ intersegmental hopping ($r_{\mathrm{intersegment\ hop}} = 0$ in Figure 9b) clearly predicts much higher probability of long residence times. Reduction of the intersegmental jump rate to $r_{\mathrm{intersegment\ hop}} = 0.023\ \mathrm{ns}^{-1}$ (by a factor of 2 from $r_{\mathrm{intersegment\ hop}} = 0.047\ \mathrm{ns}^{-1}$) leads to a noticeably slower decay of the EO−Li^+ residence time ACF for $t > 10$ ns that the ACF. Analysis of Li^+ diffusion along a chain indicates that it travels on average from 11 to 16 PEO repeat units before it undergoes an intersegmental jump with the longer distances corresponding to low salt concentration.

We are ultimately interested not in the Li^+ diffusion along PEO but in the contribution of this mechanism to Li^+ displacement in the SPEs. A relationship between the average physical distance between any atoms i and j (R_{ij}) of the same PEO chain and the number of bonds ($|i - j|$) comprising the chain segment between these atoms needs to be established in order to convert

Table 2. Parameters for the Microscopic Model of Li^+ Transport[a]

salt conc. (EO:Li)	temp (K)	***a*** coeff from the $at^{0.6}$ fit to the Li^+ MSD together with a PEO segment ($Å^2\ ps^{-0.6}$)	diffusion coeff along PEO chains $(repeat\ units)^2/ns$	length of intersegmental jump (Å)
39	423	0.783	9.50	5.8
20	423	0.580	9.50	5.8
20	393	0.350	5.10	7.0
10	423	0.488	7.00	5.8
7.5	423	0.396	6.00	5.0

[a] The rate of intersegmental jumps and fraction of free ions are shown in Table 1.

the number of repeat units a Li^+ traveled with its mean-squared displacement. For this purpose we utilize the relationship

$$\langle R_{ij}^2 \rangle = C|i - j|l^2 \tag{7}$$

where l^2 is the mean-squared bond length (2.07 $Å^2$) and C_n ($n = |i - j|$) is the characteristic ratio of PEO that depends relatively weakly upon both n and salt concentration. We have shown previously that characteristic ratio decreases with increasing salt concentration;[37] we observed the same tendency here as well. C_n as a function of n calculated eq 7 was used in a model to obtain lithium mean-squared displacements for its diffusion along PEO.[38] As Li^+ diffusion along a polymer yields the number of bonds Li^+ traveled $n \sim t^{0.5}$, one obtains from eq 7 that Li^+ diffusion along an infinitely long PEO chain is subdiffusive with MSD $\sim t^{0.5}$ at the limit of long times.

The motion of Li^+ together with a polymer segment and the distance a Li^+ travels when it undergoes an intersegmental hop are additional quantities needed for the macroscopic model that can be extracted from molecular dynamics simulations. We found that when a cation is complexed by a PEO segment that during the time during which its coordination does not change the cation motion can be described as MSD(t) = $at^{0.6}$. This scaling corresponds to that observed for monomers in the subdiffusive regime in numerous simulations of polymer melts.[39] Table 2 summarized the a coefficient (from $at^{0.6}$) obtained from and fits to MD data.

Finally, the length for the intersegmental hops was estimated from the difference between the MSD for the Li^+ that undergoes intersegmental jumps minus the MSD for the Li^+ that does not undergo any intersegmental hops and only moves together with and/or along a PEO chain. The intersegmental hop lengths were found in the range from 5 to 8 Å. The electrolytes at lower temperatures and lower salt concentrations tend to have longer intersegmental jump lengths. Note that our estimates of the intersegmental jump length are similar to the value of 7 Å found in ab initio quantum chemistry studies of the intersegmental Li^+ transfer between two PEO segments.[40] The intersegmental hopping lengths used in the microscopic model are given in Table 2.

Simulations of a Li^+ diffusion using developed microscopic model with parameters given in Table 2 yielded total Li^+ MSD-(t) shown in Figure 11. Good agreement between model predictions and simulation data is observed. We would like to point out that the Li^+ MSD from the model exhibits a subdiffusive behavior for times shorter than an average intersegmental hopping time and crosses over to the diffusive regime after than.

Having validated this microscopic model, we can analyze in detail the contributions of each mechanism to cation diffusion. We have examined four scenarios of Li^+ diffusion: (a) Li^+ moves with PEO segments and along PEO chains but no intersegmental hopping is allowed; (b) Li^+ moves with PEO segments and undergoes intersegmental hops, but no movement along PEO chains is allowed; (c) Li^+ moves only along PEO chains and undergoes intersegmental hops, but no movement with PEO segments is allowed; (d) Li^+ moves only by intersegmental hops with no motion along PEO or with PEO segments. For scenario (a), the Li^+ diffusion coefficient is equal to the diffusion coefficient of the host polymer chains, which is essentially zero for high molecular weight entangled or cross-linked polymers. The diffusion coefficients obtained from the microscopic model for the latter three scenarios are shown in Figure 12. At low salt concentrations the contribution from Li^+ diffusion along PEO chains to total Li^+ diffusion is approximately equal to the contribution from Li^+ diffusion together with a PEO segment. As salt concentration increases the contribution from cation diffusion along PEO chains decreases more rapidly than that from Li^+ diffusion with a PEO segment because fewer coordinating sites (free EO) are available for the cation, thereby increasing the need for coordinated cation motion along the polymer chain. Finally, if only intersegmental hops are allowed for the Li^+ diffusion, the diffusion coefficient is ≈10% of the magnitude of the total diffusion coefficient, indicating that displacement of the cation by Li^+ motion along PEO and/or with PEO segments between segmental hops is also essential for achieving fast Li^+ transport.

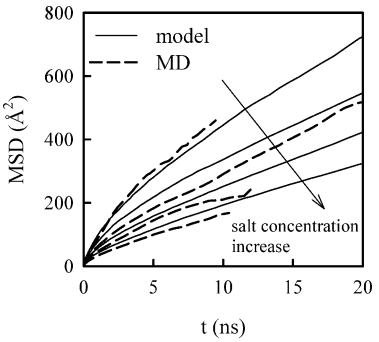

Figure 11. Li^+ mean-square displacement (MSD) calculated directly from MD simulations and the microscopic model for Li^+ transport for EO:Li = 39, 20, 10, and 7.5 at 423 K.

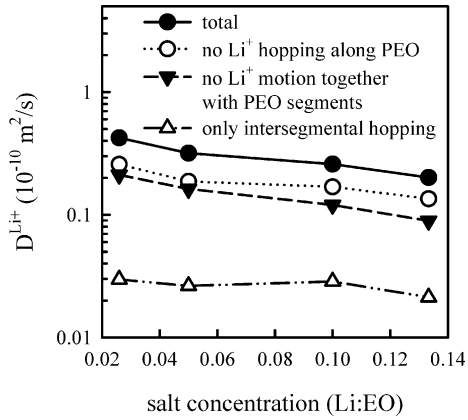

Figure 12. Macroscopic Li^+ diffusion coefficient from the model with various contributions to the Li^+ transport included for EO:Li = 20 salt concentration.

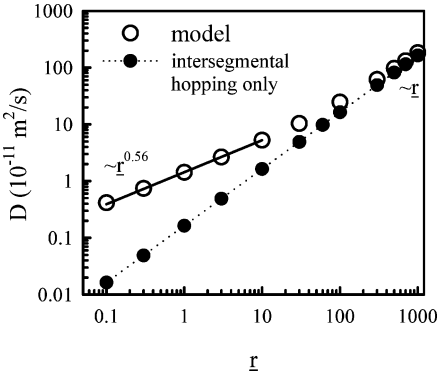

Figure 13. Dependence of the Li^+ diffusion coefficient on the reduced intersegmental hopping rate (**r**), $\mathbf{r} = r/r$(for EO:Li = 20 at 393 K) for the microscopic model. The Li^+ diffusion occurring only by intersegmental hopping without motion with or along PEO is also shown.

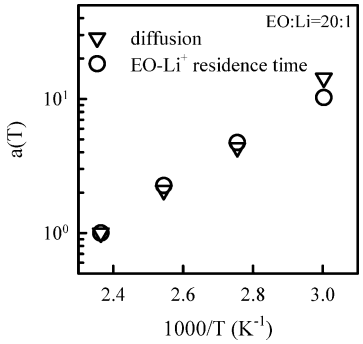

Figure 14. Shift factor $a(T)$ accounting for temperature dependence of the Li^+ self-diffusion coefficient and EO−Li^+ residence times.

It is instructive to analyze the influence of the intersegmental hopping rate on Li^+ motion in a limit of high molecular weight PEO chains in the amorphous phase. Figure 13 shows Li^+ diffusion coefficient predicted by the microscopic model for EO:Li = 20 at 393 K as a function of the reduced intersegmental hopping rate (r), where r represents an increase or decrease of the hopping rate relative to the original model parameters. Our model assumes that the mean intersegmental hopping time is smaller than the Rouse time of the chain, or for entangled chains, the Rouse time associated with the entanglement molecular weight, allowing us to utilize $\mathrm{MSD}(t) = at^{0.6}$ for displacements associated with motion with PEO segment. We observed that the Li^+ diffusion coefficient scales at $\sim r^{0.56}$ in the region near the $r = 1$. An increase of the intersegmental hopping rate by more than 2 orders of magnitude results in more than half of Li^+ transport occurring by intersegmental jumps. In this regime when intersegmental hopping dominates Li^+ diffusion, scaling changes to $D \sim r$, as seen from Figure 13.

At the final stage of our analysis of the Li^+ transport mechanism, the temperature dependence of the EO−Li^+ residence time reflecting the Li^+ diffusion along PEO and intersegmental hops is compared with the shift factor for the overall Li^+ diffusion coefficient as a function of temperature (Figure 14). A similar temperature dependence of these two processes indicates that the mechanisms of the Li^+ transport investigated at high temperature are similar at low temperatures.

VI. Conclusions

MD simulations with the recently developed quantum-chemistry-based many-body polarizable force field demonstrated excellent predictive capabilities of the method and provided reliable Li^+ local environment, extent of ion aggregation, ion and polymer diffusion coefficient, and conductivity over a broad range of salt concentrations and temperatures. Because of the extensive validation, we have significant confidence in the mechanisms of ion transport observed in our simulations.

We found that the Li^+ transport arises from a combination of a subdiffusive Li^+ motion along PEO chains (MSD $\sim t^{0.5}$), a Li^+ motion together with PEO segments (MSD $\sim t^{0.6}$ for $t <$ Rouse time), and Li^+ intersegmental hopping from one PEO segment to another. A Li^+ moves 11−14 PEO repeat units on average in between intersegmental hops. At low salt concentrations (EO:Li < 20) Li^+ hopping along PEO chains has a similar contribution to the overall Li^+ transport as a Li^+ transport together with PEO segments. Lithium intersegmental hops are central to viable Li^+ transport because without them the lithium diffusion coefficient would be equal to that of PEO chains. The rate of intersegmental hops was ≈0.05 and ≈0.02 ns^{-1} at 423 and 393 K, respectively, correlating well with times, where lithium motion undergoes a crossover from the subdiffusive to the diffusive regime.

The concentration dependence of the local relaxation of PEO segments is very similar to the concentration dependence of the Li^+ and $TFSI^-$ self-diffusion coefficients, indicating that local polymer relaxation is coupled with dynamics of both Li^+ and $TFSI^-$. We have further confirmed coupling of the PEO conformational dynamics with the transport of both Li^+ and $TFSI^-$ ions by raising barriers for PEO conformational transition that decreased the polymer segmental dynamics, Li^+ and $TFSI^-$ diffusion to the same extent, confirming that dynamics not only of Li^+ but also of a relatively large $TFSI^-$ anion is also coupled to the polymer segmental relaxation.

Acknowledgment. The authors are indebted to a subcontract from LBL #6515401 and NASA (grant NAG3 2624) for financial support.

References and Notes

(1) Yamaki, J.; Tobishima, S. Rechargeable Lithium Anodes. In *HandBook of Battery Materials*; Besenhard, J. O., Ed.; Wiley-VCH: New York, 1999.
(2) Gray, F. M. *Polymer Electrolytes*; The Royal Society of Chemistry: Cambridge, 1997.
(3) Thomas, K. E.; Sloop, S. E.; Kerr, J. B.; Newman, J. *J. Power Sources* **2000**, *89*, 132.
(4) Wilson, D. J.; Nicholas, C. V.; Mobbs, Ri. H.; Booth, C.; Giles, J. R. M. *Br. Polym. J.* **1990**, *22*, 129.
(5) Buriez, O.; Han, Y. B.; Hou, J.; Kerr, J. B.; Qiao, J.; Sloop, S. E.; Tian, M.; Wang, S. *J. Power Sources* **2000**, *89*, 149.
(6) Soo, P. P.; Huang, B.; Jang, Y.-I.; Chiang, Y.-M.; Sadoway, D. R.; Mayes, A. M. *J. Electrochem. Soc.* **1999**, *146*, 32.
(7) Allcock, H. R.; Napierala, M. E.; Olmeijer, D. L.; Cameron, C. G.; Kuharcik, S. E.; Reed, C. S.; O'Connor, S. J. M. *Electrochim. Acta* **1998**, *43*, 1145.
(8) Bruce, P. G.; Vincent, C. A. *J. Chem. Soc., Faraday Trans* **1993**, *89*, 3187.
(9) Croce, F.; Curini, R.; Martinelli, A.; Persi, L.; Ronci, F.; Scrosati, B.; Caminiti, R. *J. Phys. Chem. B* **1999**, *103*, 10632.
(10) Scrosati, B.; Croce, F.; Persi, L *J. Electrochem. Soc.* **2000**, *147*, 1718.
(11) Borodin, O.; Smith, G. D. *Macromolecules* **2000**, *33*, 2273−2283.
(12) Müller-Plathe, F.; W. F. van Gunsteren *J. Chem. Phys.* **1995**, *103*, 4745.
(13) Neyertz, S.; Brown, D. *J. Chem. Phys.* **1996**, *104*, 3797.
(14) Borodin, O.; Smith, G. D.; Douglas, R. *J. Phys. Chem. B* **2003**, *107*, 6824.
(15) Siqueira, L. J. A.; Ribeiro, M. C. C. *J. Chem. Phys.* **2005**, *122*, 194911.
(16) Duan, Y. H.; Halley, J. W.; Curtiss, L.; Redfern, P. *J. Chem. Phys.* **2005**, *122*, 054702.
(17) Mos, B.; Verkerk, Pouget, S.; van Zon, A.; Bel, G.-J.; de Leeuw, S. W.; Eisenback, C. D. *J. Chem. Phys.* **2000**, *113*, 4.
(18) Borodin, O.; Smith, G. D. *J. Phys. Chem. B*, submitted for publication.
(19) Lucretius, www.che.utah.edu/~gdsmith.
(20) Martyna, G. J.; Tuckerman, M.; Tobias, D. J.; Klein, M. L. *Mol. Phys.* **1996**, *87*, 1117.
(21) Ryckaert, J. P.; Ciccotti, G.; Berendsen, H. J. C. *J. Comput. Phys.* **1977**, *23*, 327.

(22) Steinhauser, O. *Mol. Phys.* **1982**, *45*, 335.
(23) Martyna, G. J.; Tuckerman, M.; Tobias, D. J.; Klein, M. L. *Mol. Phys.* **1996**, *87*, 1117.
(24) Edman, L. *J. Phys. Chem. B* **2000**, *104*, 7254−7258.
(25) Moa, G.; Saboungi, M.-L.; Price, D. L.; Armand, M. B.; Howells, W. S. *Phys. Rev. Lett.* **2000**, *84*, 5536.
(26) 2.8 Å is the position of the minimum after the first peak of the Li−O radial distribution function.
(27) Christie, A. M.; Lilley, S. J.; Staunton, E.; Andreev, Y. G.; Bruce, P. G. *Nature (London)* **2005**, *433*, 50.
(28) MacGlashan, G. S.; Andreev, Y. G.; Bruce, P. G. *Nature (London)* **1999**, *398*, 792.
(29) Stoeva, Z.; Martin-Litas, I.; Staunton, E.; Andreev, Y. G.; Bruce, P. G. *J. Am. Chem. Soc.* **2003**, *125*, 4619.
(30) Hayamizu, K.; Akiba, E.; Bando, T.; Aihara, Y. *J. Chem. Phys.* **2002**, *117*, 5929.
(31) Edman, L.; Ferry, A.; Oradd, G. *Phys. Rev. E* **2002**, *65*, 042803.
(32) Edman, L.; Doeff, M. M.; Ferry, A.; Kerr, J.; De Jonghe, L. C. *J. Phys. Chem. B* **2000**, *104*, 3476−3480.
(33) Gusev, A. A.; Müller-Plather, F.; van Gunstern, W. F.; Suter, U. W. *Adv. Polym. Sci.* **1994**, *116*, 207.
(34) Müller-Plather, F. *Acta Polym.* **1994**, *45*, 259.
(35) Hahn, O.; Mooney, D. A.; Müller-Plathe, F.; Kremer, K. *J. Chem. Phys.* **1999**, *111*, 6061.
(36) Lascaud, S.; Perrier, M.; Vallee, A.; Besner, S.; Prud'homme, J.; Armand, M. *Macromolecules* **1994,** *27*, 7469−7477.
(37) Annis, B. K.; Kim, M. H.; Wignall, G. D.; Borodin, O.; Smith, G. D. *Macromolecules* **2000**, *33*, 7544.
(38) For very local Li^+ displacements of four repeat units or less along a PEO chain we modeled Li^+ displacement as hopping a distance of 2.9 Å per repeat unit corresponds to the O···O distance in the PEO most probable trans−gauche−trans conformation around a −O−C−C−O− torsional triad.
(39) Paul, W.; Smith, G. D. *Rep. Prog. Phys.* **2004**, *67*, 1117.
(40) Curtiss, L., private communication.

MA052277V